PCCP

ROYAL SOCIETY OF CHEMISTRY

PAPER

View Article Online
View Journal | View Issue

Cite this: *Phys. Chem. Chem. Phys.*, 2020, **22**, 25492

Increasing the weights in the molecular work-out of *cis*- and *trans*-formic acid: extension of the vibrational database *via* deuteration†

Arman Nejad, Martin A. Suhm and Katharina A. E. Meyer *

Received 22nd August 2020,
Accepted 2nd November 2020

DOI: 10.1039/d0cp04451b

rsc.li/pccp

The higher-energy *cis*- as well as the global minimum *trans*-rotamers of the four H/D isotopologues of the formic acid monomer have been examined with Raman jet spectroscopy extending the vibrational gas phase reference database by eleven new *cis*-band positions for HCOOD, DCOOH, and DCOOD. With these new additions, all O–H/D, C–H/D, and C=O stretching as well as the O–D in-plane bending vibrations of these higher-energy rotamers are known in addition to the previously determined C–O stretch and OH torsion of *cis*-HCOOH. Further, a comparison of the vibrational spectra of all four H/D isotopologues of the globally stable *trans*-rotamer of formic acid is shown to be very helpful in revealing similarities and differences in these systems, particularly with regard to Fermi resonances. Amongst the most prominent ones is the $\nu_5/2\nu_9$ resonance doublet of *trans*-HCOOH, for which we provide more insight into a recently suggested label switch of the resonance partners *via* the comparison of infrared and Raman jet spectra.

1 Introduction

As an important contributor to atmospheric chemistry,[1,2] the formic acid monomer, particularly its global minimum *trans*-conformation, has received much attention over the years both from the experimental[3–10] as well as the theoretical[11–13] side. Despite the low abundance of merely 0.1% at room temperature, the first gas phase detection of the higher-energy *cis*-conformer was achieved with microwave spectroscopy in 1976 by Hocking,[14] enabled by the threefold larger dipole moment of *cis*- (3.79 D) compared to *trans*-HCOOH (1.42 D).[15] The first vibrational characterisation of *cis*-formic acid was accomplished in 1997 for HCOOH in an argon matrix *via* OH overtone excitation from the global minimum *trans*-rotamer[16] and was subsequently extended to DCOOH[17] and HCOOD.[18,19] For a direct comparison to theory,[20] however, these values are not so practical, as the host–guest interaction needs to be captured on the theoretical side which can be challenging, as recently shown by Ito for the formic acid dimer.[21] The first and until 2018 only *cis*-formic acid fundamental measured in the gas phase was the OH torsion connecting both minima[22] – the vibrational mode with the largest (predicted) spectral separation between both conformers. Four new band positions of *cis*-HCOOH have been determined in 2018 and 2019 with Raman jet spectroscopy, utilising thermal excitation to increase the *cis*-formic acid abundance by an order of magnitude[23,24] prior to the expansion. Here, we present the first perturbation-free band positions of partially and fully deuterated *cis*-formic acid, extending the available *cis*-database by more than 200% from five to sixteen fundamentals. In 2019, *cis*-formic acid has also been detected as a distinct species in solution,[25] where it has a much higher abundance than in the gas phase. The O–D and C=O stretches were shown to be higher in frequency than those in the *trans*-form, as observed here under vacuum isolation, but only in weakly hydrogen-bonded solvents. In water, the sequence inverts for the O–D stretch, underscoring the importance of reliable reference values in the gas phase for theory.

Despite the completion of the vibrational gas phase database for the *trans*-rotamers of the H/D isotopologues of formic acid (with the exception of ν_8 of HCOOD), there is still ambiguity in the assignment of Fermi resonance pairs. One prominent example is the $\nu_5/2\nu_9$ Fermi resonance of *trans*-HCOOH. This resonance is part of a larger resonance polyad involving half a dozen of states[26] and problems with the ν_5 assignment were noted early on. In 2019, Hull *et al.* presented convincing experimental evidence that the overtone $2\nu_9$ is – contrary to previous beliefs – lower in energy than the fundamental ν_5,[27] in agreement with recent high-level calculations.[11,12]

As we will highlight in this contribution, one of the most crucial and insightful aspects that improves our understanding

Institute of Physical Chemistry, University of Göttingen, Tammannstr. 6, 37077 Göttingen, Germany. E-mail: katharina.meyer@chemie.uni-goettingen.de

† Electronic supplementary information (ESI) available: *cis*-Formic acid spectra, comparison of formic acid vibrational nomenclature, harmonic avoided crossing calculated at other levels than B3LYP-D3, as well as computational raw data and further experimental details. See DOI: 10.1039/d0cp04451b

of near-degeneracies in these systems is the comparison of vibrational spectra of all four H/D isotopologues. The work of Redington, who has analysed 24 isotopologues of the formic acid monomer in a neon matrix,[28] is an impressive example of such rigorous comparison. Further, we showcase the indispensability of Raman spectroscopy for a thorough vibrational characterisation of the formic acid monomer, which is so far underrepresented[4,5,23,24,29–31] in comparison to a wealth of infrared studies (see for example ref. 3, 6–10, 32–41 and references therein). We extend and update the significant Raman gas phase work on hydrogenated and deuterated formic acid by Bertie *et al.*,[4,5] which was focussed on the characterisation of the dimer.

From a computational point of view, the small size of only five atoms and two conformational isomers (energy difference of 16.3(4) kJ mol^{-1} (ref. 14)) makes the formic acid monomer particularly suitable for benchmarking quantum chemical models. The availability of benchmarking data in higher-energy regimes of the potential energy hypersurface (PES), *e.g.*, local minima, is especially important, as it enables the assessment of the globality of the PES description. The need for higher-energy reference data is illustrated by two recent high-level variational anharmonic calculations, namely vibrational configuration interaction (VCI)[11] and multi-configuration time-dependent Hartree (MCTDH),[12] where the mean absolute deviation (MAD) between both models is 4 cm^{-1} for the global minimum *trans*-, but nearly three times as large (12 cm^{-1}) for the *cis*-conformer. For *trans*-HCOOH, all nine fundamentals were considered for this analysis, but for the higher-energy *cis*-rotamer only eight, as ν_1 was not reported in ref. 11. Another excellent test to reveal weaknesses in theoretical models are near-degeneracies, as recently showcased for the glycolic acid monomer,[42] and extended in this work to the *trans*-rotamer of the formic acid monomer. A full characterisation of the rotational and vibrational states of *cis*- and *trans*-formic acid, which contribute to their partition function, together with an independent experimental value of the equilibrium constant between the two species could provide a more accurate experimental value for the energy difference between the two species,[43] which so far relies on a single microwave analysis.[14]

2 Experimental and computational methods

The Raman jet set-up used to record all spectra has been described in detail before.[24,44,45] Briefly, formic acid was seeded into helium and expanded at different temperatures through a vertical slit nozzle at 0.5 bar into an evacuated jet chamber (background pressures of 1–2 mbar during the expansion). Before the expansion, the acid-in-helium mixture was further diluted with helium yielding acid concentrations of $<$0.2–0.4% (Table S1 in the ESI†). Both the nozzle and its feed-line are heatable, which can be exploited to enhance the relative population of higher-energy conformers before the expansion,[24] while cluster formation is suppressed. To ensure stable conditions during the long exposures needed for the low spontaneous Raman scattering photon flux, the gas expansion is continuous (see ref. 45 for further details). A 25 W continuous-wave Spectra Physics Millennia eV 532 nm laser was used to probe the expansion. For the HCOOD measurements, a slightly lower laser power of 24 W was employed. The distance between the slit nozzle and the laser beam was set to 1 mm. The scattered light was collected perpendicular to the laser and to the nozzle flow *via* a camera lens and focussed onto a 1 m monochromator (McPherson) which disperses the photons onto 1340 pixel columns of a 1340 $\times$ 400 liquid nitrogen-cooled CCD-camera (Princeton Instruments, PyLoN 400B), that was operated in vertical binning mode (400 pixels). The combination of laser and monochromator results in a resolution of about 1.5–2.0 cm^{-1}, depending on the spectral range. Therefore, we generously assign band centre errors of $\pm$2 cm^{-1}. Exposure times of 200–300 s were used per scan and typically 5–9 scans were co-added for each spectral window. To calibrate the raw spectra in the wavenumber domain, neon lines were measured and compared to the known vacuum transitions in the NIST database. Spikes due to cosmic rays were eliminated by comparing multiple exposures for the same pixel column.

The FTIR jet spectra were recorded with a Bruker IFS 66v spectrometer equipped with a globar, a potassium bromide beam splitter, and potassium bromide optics. The modulated IR beam is gently focussed on the pulsed jet expansion from a 600 $\times$ 0.2 mm^2 slit nozzle. Behind it, the beam is focussed onto a mercury cadmium telluride (MCT) detector. A comparison of the expansion conditions of the FTIR and Raman set-up can be found in ref. 46 and further details on the FTIR set-up in ref. 47.

Geometry optimisations and the calculation of harmonic vibrational frequencies, IR intensities, and Raman activities have been performed with Gaussian 09 Rev. E.01.[48] Keyword specifications for all calculations are summarised in the ESI† (Table S2). From the computed Raman activity A_i, the Raman scattering cross-section σ_i was calculated as

$$\sigma_i = \frac{2\pi^2 h}{45 c \omega_i} \cdot \frac{\tilde{\nu}_{\text{Laser}} (\tilde{\nu}_{\text{Laser}} - \omega_i)^3}{1 - \exp\left(-\frac{hc\omega_i}{k_B T_{\text{vib}}}\right)} \cdot g_i A_i, \quad (1)$$

where $\tilde{\nu}_{\text{Laser}}$ = (532 nm)$^{-1}$ is the laser wavenumber, T_{vib} the vibrational temperature, ω_i the harmonic wavenumber, g_i the degeneracy of the vibration, and c the speed of light in vacuum. To roughly match the vibrational temperature in our jet, a temperature of 100 K was assumed in all our calculations.

For spectral assignments, the B3LYP functional[49,50] was employed using two-body dispersion corrections (D3),[51] Becke–Johnson damping,[52] and the aug-cc-pVTZ basis set,[53] hereafter denoted as aVTZ. All harmonic vibrational frequencies were scaled to the respective *trans*-formic acid band in each spectral window and in case of Fermi resonances, to the resonance centre ascertained from the overall scattering intensity. A list of the calculated harmonic vibrational frequencies, IR intensities, and Raman scattering cross-sections can be found in Table S3 in the ESI.†

In order to analyse harmonic mode mixing (see Section 3.3), additional harmonic vibrational frequency calculations were carried out at the PBE0-D3(BJ),[54] B2PLYP-D3(BJ),[55] HF, MP2[56] (all Gaussian 09 Rev. E.01[48]), and CCSD(T)[57] levels (Cfour version 1[58,59]).

3 Results and discussion

3.1 *cis*-Formic acid fundamentals

To detect the *cis*-conformers of DCOOH, HCOOD, and DCOOD, Raman jet spectroscopy has been exploited in combination with thermal excitation between 100 and 190 °C utilising a heatable nozzle and feed-line, followed by a supersonic expansion to rapidly freeze out the enhanced *cis*-population[24] of up to 1–2%. This technique is a variant of earlier trapping methods[60] with the advantage that the trapped species are generated in a state which is easily accessible to quantum chemical modelling. By intensity-scaling the spectra of a temperature series to the respective *trans*-fundamental in each spectral region, *cis*-formic acid bands and non-isomeric hot bands, *i.e.*, transitions from thermally populated states localised in *trans*-formic acid, can be easily distinguished from cold monomer and cluster bands, as they increase in intensity with temperature, whereas the cluster bands decrease. An illustrative example of this can be seen in the ν_2 spectra of HCOOH in Fig. S3 in the ESI.†

There are two measures to identify the molecular origin of a hot band – the band position difference to the *trans*-fundamental and the intensity. In the perturbational picture,[61] the spectral shift between a fundamental ν_i and the hot band $\nu_i + \nu_j - \nu_j$ amounts to the anharmonic matrix element x_{ij} ($2x_{ii}$ for $2\nu_i - \nu_i$), which mediates binary coupling between two vibrational modes i and j (diagonal anharmonicity along mode i). The intensity of a non-isomeric hot band can be estimated from the expected Boltzmann population of that low-lying energy level j assuming similar Raman scattering cross-sections (see ref. 24 for further details). In case of an isomeric hot band, the expected population can be estimated from the energy difference between both conformers (1–2% at 190 °C[24]) and the difference in band position corresponds to the *cis*–*trans*-shift.

Fig. 1 shows the normalised relative Raman scattering cross-sections for all four H/D isotopologues and both rotamers of formic acid, indicating which vibrations are accessible with our experimental approach. For reasons of simplification and unification, we employ the Herzberg nomenclature of HCOOH for all isotopologues and rotamers (see Table S4 in the ESI† for comparison).

As for HCOOH,[24] the most Raman active modes of the deuterated isotopologues are the O–H/D, C–H/D, and C=O stretches (ν_1–ν_3), for which all missing *cis*-fundamentals were determined in this work. We note that the assignment of ν_2 of *cis*-DCOOH is somewhat tentative due to the prominent rovibrational and hot band structure of the respective *trans*-band (*cf.* Fig. S3 in the ESI†). The same applies to ν_6 of *cis*-HCOOH.[62] Due to the abundance disadvantage of *cis*-formic acid, most of the remaining *cis*-fundamentals are more difficult to access with our experimental approach. The notable exception is the O–D in-plane bending vibration ν_5 of HCOOD and DCOOD. For other *cis*-fundamentals with seemingly high intensity such as ν_4 and ν_6 of DCOOH (*cf.* Fig. 1), spectral congestion due to an excessive hot band structure currently limits further conclusions. Guidance from theory would be particularly helpful for these spectral regions. ν_8 and ν_9 are close to the detection limit for the *trans*-rotamer, and below it for the *cis*-rotamer impurity.

A list of all available hydrogenated and newly determined deuterated (perturbation-free) *cis*-fundamentals of the formic

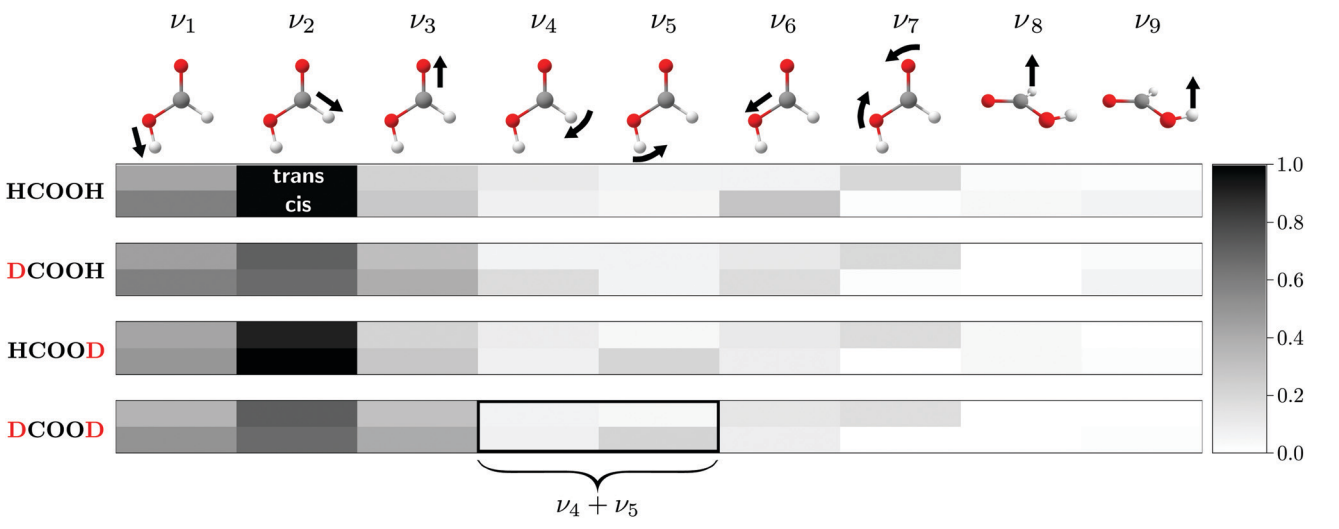

Fig. 1 Harmonic (B3LYP-D3(BJ)/aVTZ) Raman scattering cross-sections of the formic acid monomer for both rotamers of all four H/D isotopologues, normalised to ν_2 of HCOOD (scaling factor 175.9 × 10^{-36} m^2 sr^{-1}). A darker grey tone for the *cis*-rotamer indicates higher visibility than for the *trans*-rotamer, but the lower *cis*-abundance in the experiment must be kept in mind. The normal modes of *cis*-formic acid are visualised by arrows and labelled according to the Herzberg nomenclature for HCOOH, which is adopted for the deuterated isotopologues. For ν_4 and ν_5 of DCOOD, harmonic mode mixing into a symmetric and antisymmetric combination is predicted. See text for further details.

Table 1 Raman jet (Ra. jet) band positions (in cm^{-1}) of *cis*- and *trans*-formic acid and their deuterated isotopologues in comparison to literature values. Fermi resonance doublets are indicated by braces. Assignments which are somewhat tentative due to overlapping hot band and/or rovibrational structure are italicised (see text for discussion and ref. 62)

	HCOOH			DCOOH			HCOOD			DCOOD		
	Ra. jet	Lit.		Ra. jet	Lit.		Ra. jet	Lit.		Ra. jet	Lit.	
cis												
ν_1	3637		[a]	3635			2685			2685		
ν_2	2873		[a]	*2167*			2871			2145		
ν_3	1818		[a]	1790			1819			1789		
ν_5							904			883		
ν_6	*1093*		[a]									
ν_9		493.42	[b]									
trans												
ν_1	3570 / 3567	3570.5	[c]	3569	3566	[i]	2631	2631.64	[o]	2632	2631.87	[t]
ν_2	2942	2942.06	[c]	2219	2219.69	[j]	2954 / 2938	2938.2	[i]	2231 / 2194	2231.8 / 2195.1	[u] [u]
ν_3	1776	1776.83	[d]	1762 / 1725	1762.9 / 1725.87	[k] [k]	1772	1772.12	[p]	1761 / 1725	1760.0 / 1725.12	[u] [v]
ν_4	1379	1379.05	[e]	971	970.89	[l]	1365	1366.48	[e]	1039	1042	[u]
ν_5 / $2\nu_9$	1306 / 1220	1306.2 / 1220.83	[c] [f]	1299 / 1206	1297	[i]	972 / 1010	972.85 / 1011.68	[q] [q]	945	945.0	[u]
ν_6	1104	1104.85	[g]	1142	1142.31	[m]	1176	1177.09	[r]	1170	1170.80	[w]
ν_7	626	626.17	[h]	620	620.57	[n]	558	558.27	[s]	554	554.44	[s]
ν_8		1033.47	[g]		873.39	[l]					873.2	[x]
ν_9		640.73	[h]		631.54	[n]		508.13	[s]		492.23	[s]

[a] Ref. 23 and 24. [b] Ref. 22. [c] Ref. 6; the band listed for ν_5 was originally assigned to $2\nu_9$. [d] Ref. 40 and 63. [e] Ref. 10. [f] Ref. 9; the band was originally assigned to the fundamental ν_5. [g] Ref. 64. [h] Ref. 8 and 39. [i] Ref. 5; the second band of the ν_2 resonance doublet is reported at 2941.8 cm^{-1}, but corresponds to an impurity of HCOOH in the spectra and is therefore not listed here. [j] Ref. 37. [k] Ref. 65. [l] Ref. 66. [m] Ref. 67. [n] Ref. 68. [o] Ref. 69. [p] Ref. 70, see also ref. 71 and 72. [q] Ref. 73. [r] Ref. 74. [s] Ref. 36. [t] Ref. 75. [u] Ref. 4. [v] Ref. 7. [w] Ref. 76. [x] Ref. 33.

acid monomer can be found in Table 1 alongside the corresponding *trans*-bands and high resolution literature values wherever available. A detailed view of the *cis*-formic acid spectra can be found in the ESI† (Fig. S2–S5). The agreement between the newly determined Raman jet and literature band positions for *trans*-formic acid is generally within the experimental uncertainty of our set-up (± 2 cm^{-1}, *cf.* Section 2). A preliminary Raman jet study from our laboratory[31] generally agrees with the *trans*-formic acid results reported here, within the previous, somewhat larger calibration error and apart from a few assignments. For *cis*-formic acid, the vibrational reference database has been extended by eleven new band positions. With one gas phase band position[22] and four Raman jet values from previous studies[23,24] for *cis*-HCOOH, the total number of *cis*-formic acid fundamentals now amounts to sixteen.

A recent example of a high-level variational anharmonic *ab initio* study on the formic acid monomer is an MCTDH study by Aerts *et al.* from 2020[13] who have characterised the *cis*- and *trans*-conformers of all three deuterated isotopologues. Due to the lack of environment-free experimental data on the higher-energy structure, the accuracy of their description could solely be evaluated for the global minimum *trans*-form. The new *cis*-formic acid band positions reported in this work also facilitate a performance evaluation for the higher-energy rotamer. For most modes, the deviations are below 2–3 cm^{-1}. The largest band position discrepancy is observed for ν_1 of *cis*-DCOOH and amounts to 10 cm^{-1} followed by 9, 4, and 7 cm^{-1} for ν_3 of *cis*-DCOOH, *cis*-HCOOD and *cis*-DCOOD, respectively.

3.2 Comparison of the Raman spectra of all four H/D isotopologues

An overview of the Raman spectra of the four H/D (*trans*-)formic acid isotopologues is shown in Fig. 2 for a nozzle temperature of 160 °C – a compromise between the absence of cluster signals and signal intensity. Fermi resonance doublets of the *trans*-rotamers are indicated by brackets. Hot bands are marked by 'h' and impurities due to H/D exchange reactions and/or the manufacturing process by a double dagger. The maximum of such impurities observed in the spectra amounts to 6(2)% (see Table S1 in the ESI† for further details). To visualise and systematically analyse the spectral similarities and differences observed for the four H/D isotopologues, the *cis*–*trans*-shift is plotted against the absolute *cis*-band position for the five vibrations characterised with Raman jet spectroscopy and the sixth vibrational mode obtained from high resolution gas phase studies by Baskakov *et al.*[8,22] in Fig. 3. In case of Fermi resonances of the respective *trans*-band, the band position of both resonance partners is shown and the symbol size reflects their relative intensity. For *cis*-formic acid, no signs of resonances were observed in our spectra, but this might be attributed to the relatively low intensity governed by the low abundance in the expansion.

The absolute band positions as well as *cis*–*trans*-shifts of the O–H and O–D stretching vibrations are insensitive to C–H isotope exchange (Fig. 3). However, next to the OH stretching band of *trans*-HCOOH (3570 cm^{-1}), one fairly strong band with an intensity ratio of one third of ν_1 can be seen at 3567 cm^{-1} in

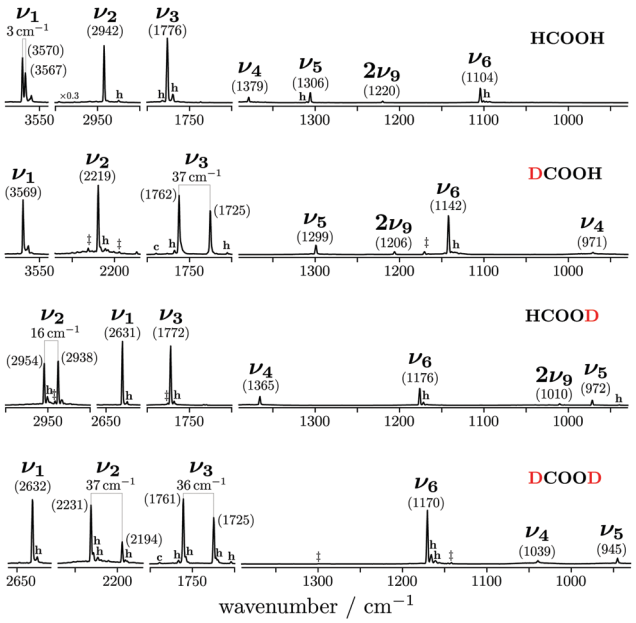

Fig. 2 Overview of the Raman jet spectra of the O–H/D, C–H/D, C=O, C–O stretching as well as C–H/D and O–H/D in-plane bending vibrations of HCOOH, DCOOH, HCOOD, and DCOOD recorded at a nozzle temperature of 160 °C. Bands of pronounced resonance doublets between fundamentals ν_i and combination or overtone bands are indicated by brackets and H, D impurities by double daggers. Non-isomeric hot and *cis*-rotamer bands are marked 'h' and 'c', respectively.

addition to a smaller third band at 3559 cm^{-1} (Fig. 2). Since the band position difference between the fundamental and the second band is very small, this does not affect the *cis–trans*-shift significantly (*cf.* Fig. 3). A similar ν_1-triad of *trans*-HCOOH has also been observed in helium nanodroplets,[38] which the authors attributed to Fermi and Coriolis resonances. For a full understanding of the OH stretching dynamics in formic acid, a detailed characterisation of skeletal modes and their associated coupling pathways is required.[77]

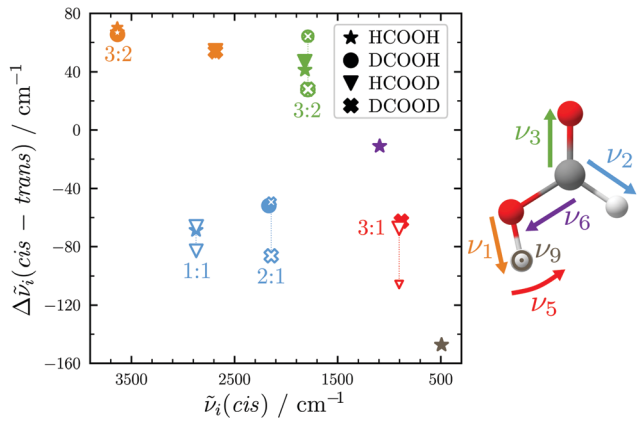

Fig. 3 *cis–trans* vibrational band position shifts plotted against the *cis*-band positions for all H/D isotopologues of the formic acid monomer. The colour illustrates the type of vibration. For Fermi resonances, unfilled symbols are used and the band positions of both resonance partners are connected by dotted lines with the symbol size representing their relative intensity.

The C=O stretch ν_3 of *trans*-DCOOH and -DCOOD has a pronounced resonance (intensity ratio 3(0.5) : 2) with the C–D out-of-plane bending vibration $2\nu_8$ (Fig. 2).[65] The *cis–trans*-shift is again very similar for all isotopologues if one compares it against the resonance centre (Fig. 3).

The situation becomes different for the C–H/D stretching vibration ν_2. For *trans*-HCOOD, Bertie *et al.* reported a resonance with the $(\nu_3 + \nu_6)$ combination band, yet assigned it to an impurity of HCOOH (2941.8 cm^{-1}) in their spectra.[5] We do, however, observe a resonance doublet with an intensity ratio close to 1 : 1 and an experimental splitting of 16 cm^{-1}. The second band of the resonance doublet at 2954 cm^{-1} (Table 1) is likely overlayed by a dimer band in the spectra of Bertie *et al.* which they report at 2951.4 cm^{-1}. The clear distinction between monomeric and dimeric contributions in the spectra *via* the temperature series is one of the advantages of the new Raman spectra reported in this work. Comparing against the resonance centre, the C–H *cis–trans*-shift is insensitive to O–H deuteration (Fig. 3). The same applies to the respective absolute *cis*-band position. The larger difference between the *cis–trans*-shifts of the C–D stretching vibrations (Fig. 3) can at least partially be ascribed to the Fermi resonance between ν_2 and the $(\nu_4 + \nu_6)$ combination band of *trans*-DCOOD.[4] Interestingly, the isotope effect on the *cis*-C–D stretch is with 22 cm^{-1} much larger than for the C–H, O–D/H stretches, where these differences only amount to $\leq$2 cm^{-1} (*cf.* Table 1). This anomaly could be a result of an anharmonic perturbation that only occurs in one O–H/D isotopologue of the *cis*-rotamer, though this remains speculative due to the low intensity of the *cis*-contributions in our spectra. Another reason for this larger difference could be a misassignment of one of the two *cis*-ν_2 bands, most likely that of *cis*-DCOOH due to the spectral congestion governed by the rovibrational structure of the *trans*-band (*cf.* Fig. S3 in the ESI†). However, the good agreement of all *cis*-ν_2 bands with the high-level prediction of Aerts *et al.*[13] (deviations below 3 cm^{-1}) does not support this conjecture. Besides, close to the *cis*-band position of *cis*-DCOOD (2145 cm^{-1}), there are no other hot bands in the DCOOH spectrum and *vice versa* (Fig. S3 in the ESI†).

Similar observations with regard to the absolute *cis*-band position as well as Fermi resonance governed difference in *cis–trans*-shift (*cf.* Table 1 and Fig. 3) apply to the O–D in-plane bending vibration ν_5. However, there is another factor that sets the *trans*- (and *cis*-)DCOOD bending vibration apart from that of the other H/D isotopologues, which can be understood by taking a closer look at the $\nu_5/2\nu_9$ Fermi resonance across all H/D isotopologues.

3.3 The $\nu_5/2\nu_9$ Fermi resonance of *trans*-formic acid

The $\nu_5/2\nu_9$ Fermi resonance is amongst the most prominent ones found for *trans*-HCOOH and involves the O–H in-plane bend ν_5 and the overtone of the large-amplitude O–H torsion $2\nu_9$ (Fig. 1). In a high resolution study of the respective hot bands in 2019, Hull *et al.* showed that the labels of the two resonance partners at 1306 cm^{-1} and at 1220 cm^{-1} need to be switched, as the overtone was shown to be lower in energy than the fundamental.[27] This Fermi resonance is also present in

trans-DCOOH as well as in *trans*-HCOOD but seemingly absent in *trans*-DCOOD. For the *cis*-conformers, this Fermi resonance is not predicted,[11–13] which makes a combination of both species valuable for vibrational benchmarking.

A more detailed view of the Raman spectra of this resonance for all four isotopologues can be found in Fig. 4, which facilitates new insight into the strength of the resonance as well as into the suggested label switch for *trans*-HCOOH. Interestingly, the higher-energy band of *trans*-HCOOH at 1306 cm^{-1} is about seven times more intense than the band at 1220 cm^{-1}, though the latter was previously assigned to the fundamental. The infrared spectra of HCOOH shown alongside the corresponding Raman spectra in Fig. 5 indicate an inverse situation where the lower energy band at 1220 cm^{-1} is more intense and the 1306 cm^{-1} band is barely visible at the employed conditions. This explains why based on solely the infrared spectra, the more intense band at 1220 cm^{-1} was previously assigned to the fundamental transition. A differing intensity ratio of a Fermi resonance in infrared and Raman spectra is rather unexpected, as usually the overtone (or combination band) is 'dark', meaning that it obtains intensity primarily *via* the anharmonic resonance with the 'bright' fundamental. As

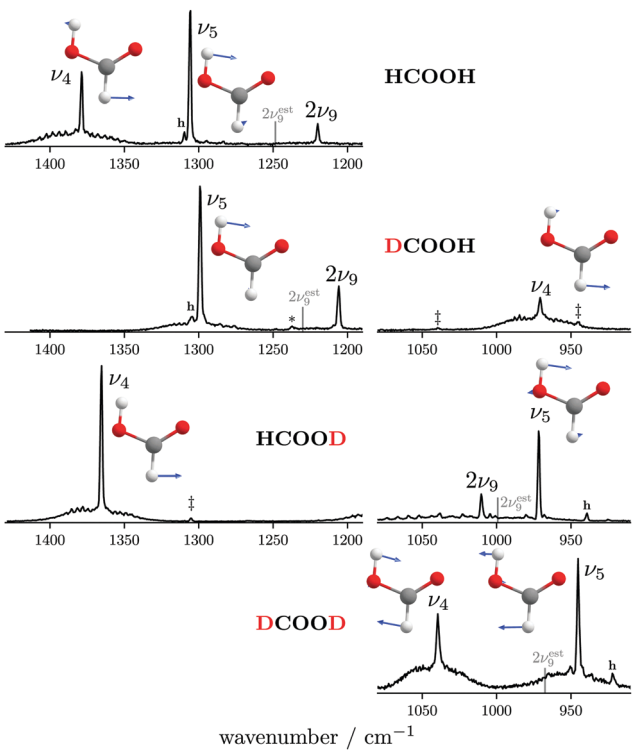

Fig. 4 Raman jet spectra of the C–H/D in-plane bending vibration ν_4 and the O–H/D $\nu_5/2\nu_9$ Fermi resonance of all four H/D isotopologues of the formic acid monomer recorded at a nozzle temperature of 160 °C. Cluster bands are marked with an asterisk, hot bands with 'h', and H, D impurities by double daggers. The band position of the overtone $2\nu_9$ has been estimated from twice the experimental band position of ν_9 (see Table 1 for band positions) by subtracting twice the diagonal anharmonicity matrix element reported in ref. 27 and is shown by a grey line. The normal modes of ν_5 and ν_4 are shown as an inset. Additional experimental details can be found in Section 2 and in the ESI.†

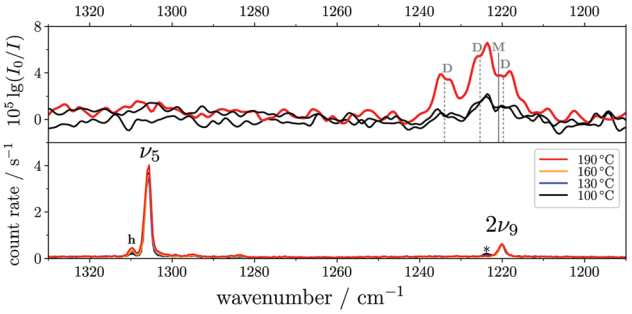

Fig. 5 FTIR (top) and Raman (bottom) jet spectra of *trans*-HCOOH in the O–H in-plane bending region (ν_5). The FTIR spectra have been recorded at increasing concentrations of <0.01–0.05% in helium at a reservoir pressure of 560 mbar with 1750–2130 co-added scans. The Raman spectra (<0.2% in helium, reservoir pressure 500 mbar, recording time 6 × 300 s) have been intensity-scaled to the ν_6 band (not shown) of *trans*-HCOOH with the lowest intensity amongst the four nozzle temperatures (100–190 °C). Assignments of monomer (M) and dimer (D) contributions to the band between 1240–1210 cm^{-1} in the FTIR spectra were taken from ref. 9. Clusters in the Raman spectrum are marked with an asterisk.

such, this infrared/Raman intensity difference implies that the overall comparably low-intense fundamental ν_5 (*cf.* Fig. 1 for relative Raman scattering cross-sections and Table S3 in the ESI† for the predicted IR intensities) 'steals' intensity from the brighter overtone in one of the spectra and the dark overtone 'steals' intensity from the brighter fundamental in the other. Considering that Raman scattering cross-sections of overtones (or combination bands) are typically about two orders of magnitude lower than those of fundamentals,[78] whereas this difference typically amounts to about one order of magnitude in the infrared, it is more plausible that the infrared ν_9 overtone is brighter than the ν_5 fundamental. This is in line with the suggested label switch of the resonance partners by Hull *et al.*,[27] which was also proposed in the VCI and MCTDH studies from 2016[11] and 2018.[12]

As aforementioned, the $\nu_5/2\nu_9$ Fermi resonance is also present in DCOOH with a slightly larger splitting (93 cm^{-1} *versus* 86 cm^{-1} for HCOOH) and a similar intensity ratio (7(2):1). In case of DCOOH, Bertie *et al.*[5] correctly assigned the band at 1299 cm^{-1} (1297 cm^{-1} in ref. 5) to the O–H in-plane bending vibration ν_5, whereas the corresponding band of HCOOH at 1306 cm^{-1} (1307 cm^{-1} in ref. 4) was assigned to $2\nu_9$ in their publication.[4] For the O-deuterated isotopologues, the $\nu_5/2\nu_9$ Fermi resonance is only observed for HCOOD, where the ν_9 overtone is higher in energy (1011.68 cm^{-1}) than the ν_5 fundamental (972.85 cm^{-1}).[73] The intensity ratio and splitting between both bands is distinctly smaller (1(1):3 *versus* 7(2):1 and 38 instead of 86/93 cm^{-1}), which is consistent with a weakening of the resonance for the smaller OD amplitudes.

The absence or at least pronounced weakness of the $\nu_5/2\nu_9$ resonance in *trans*-DCOOD (*cf.* expected band position of $2\nu_9$ in Fig. 4 which has been estimated from 2 × (ν_9) assuming an anharmonic correction of twice the anharmonicity matrix element x_{99} as reported in ref. 27) can be understood in the comprehensive analysis of all four isotopologues. Fig. 2 shows that the C–D bend of DCOOH and O–D bend of HCOOD, which are estimates for the expected band positions of ν_4 and ν_5 in

trans-DCOOD, are nearly isoenergetic at 971/972 cm^{-1}. In the DCOOD spectrum, they are shifted up (1039 cm^{-1}) and down (945 cm^{-1}) in energy, indicating harmonic mixing due to near-degeneracies. This mixing is further supported by the unusually low ratio of the Q branch with respect to the rotational contour found for ν_5 of *trans*-DCOOD (a feature of ν_4, *cf.* Fig. 4), which might result from substantial mixing with ν_4. Pointing in that same direction are different harmonic frequency calculations that unanimously predict a mixing into a symmetric and an antisymmetric combination for *cis*- and *trans*-DCOOD (HF, MP2, CCSD(T), and DFT, all with an aVTZ basis set, *cf.* inset in Fig. 4 for normal modes of the *trans*-rotamers).

For a closer scrutiny of this mixing across the four H/D isotopologues, harmonic frequencies of *trans*-formic acid were scanned for C–H proton masses between 1 and $2m(^1H)$. The harmonic wavenumbers of ν_4, ν_5, ν_6, $2\nu_7$, and $2\nu_9$ (all A′ symmetry) for both possible scans (*trans*-HCOOH → *trans*-DCOOH, *trans*-HCOOD → *trans*-DCOOD) are plotted for B3LYP-D3(BJ)/aVTZ in Fig. 6. Strong mixing between ν_4, ν_5, and ν_6 is observed in these mass-scans with avoided crossings on the order of 60–110 cm^{-1}. Accidentally, however, an avoided crossing of ν_4 and ν_5[34] coincides with an integer (even) mass in one case, *i.e.*, DCOOD. Additional scans at other levels of theory (Fig. S1 in the ESI†) show the same qualitative behaviour. As such, the potential absence of the $\nu_5/2\nu_9$ Fermi resonance in DCOOD is in part a coincidence of an avoided crossing that detunes two otherwise moderately resonant states. This alone, however, does not explain the absence of the overtone $2\nu_9$ in the DCOOD spectra entirely, as $2\nu_9$ could gain in intensity *via* coupling to ν_4 which exhibits ν_5 character. The $2\nu_9$ band of DCOOD might not gain sufficient intensity in this coupling triad to be observed under the employed experimental conditions. A comparison of measurements with perpendicular and parallel laser polarisation[78] can be used to reduce the rotational contour *via* subtraction. This depolarised spectrum of DCOOD (*cf.* Fig. S5 in the ESI†) shows that no distinct $2\nu_9$ band is hidden under the rotational contour of ν_5 of DCOOD in our spectra, providing additional affirmation of its weakness.

Overall, this harmonic mode mixing could be another reason for the differences observed for the *cis*–*trans*-shifts as well as *cis*-band positions (mixing is also predicted for *cis*-DCOOD) of HCOOD and DCOOD (Fig. 3). Subtle mass changes such as ^{13}C isotopic substitution[28] might allow for more insight, though this is experimentally too elaborate without further theoretical support.

3.4 Fermi resonance analysis for the H/D isotopologues of *trans*-formic acid

For vibrational benchmarking of near-degeneracies, not only the energetic order of the two interacting states needs to be predicted correctly by a quantum chemical model, but also their energy difference (spectral splitting $|\Delta\tilde{\nu}|$) as well as the spectral intensity ratio R (here I_{high}/I_{low}). From these two quantities, the Fermi resonance coupling constant $|W^{exp}_{Fermi}|$ can be calculated from eqn (2) under the assumption that the dark state has a negligible intensity,[79] which allows for an estimate of the strength of the resonance.

$$|W^{exp}_{Fermi}| = \frac{|\Delta\tilde{\nu}|\sqrt{R}}{(1+R)} \quad (2)$$

These effective values $|W^{exp}_{Fermi}|$ for all *trans*-formic acid Fermi resonances observed in this work are listed in Table 2 alongside model values $|W^{calc}_{Fermi}|$ calculated from a quartic force field based on the PES of Tew and Mizukami[11] (*cf.* ESI† for further details). For ν_2 of HCOOD, only the Q branches of the vibrational bands were integrated to determine $|W^{exp}_{Fermi}|$ (*cf.* Fig. S3 in the ESI†). The neglect of the overlapping rotational contours for $\nu_2/(\nu_3 + \nu_6)$ of HCOOD should not impact $|W^{exp}_{Fermi}|$ much, as the two resonance partners are nearly equal in intensity

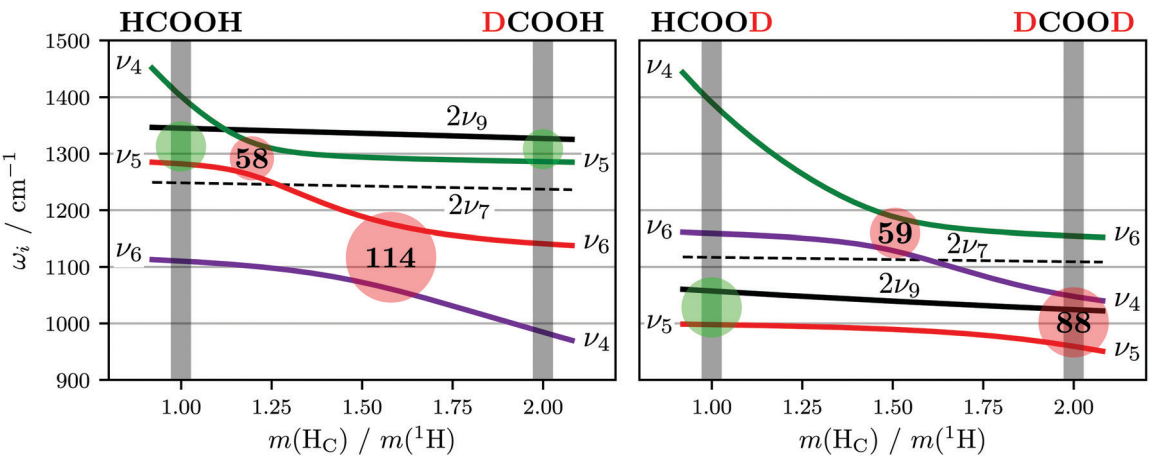

Fig. 6 Harmonic wavenumbers (in cm^{-1}, at the B3LYP-D3(BJ)/aVTZ level) of A′ symmetric fundamentals and overtones in the spectral windows between 900 and 1500 cm^{-1} as a function of the relative C–H proton mass of *trans*-formic acid (left O–H, right O–D). Grey bars indicate fractional masses which equal the mass of hydrogen or deuterium. Harmonically avoided crossing due to mode-mixing is indicated by a red disk in the interaction region, in which twice the coupling constant 2*W* is printed in bold letters. Green disks highlight the Fermi resonance-coupled states ν_5 and $2\nu_9$ in *trans*-HCOOH, -DCOOH, and -HCOOD.

Table 2 Resonance analysis for Fermi resonance split fundamentals of the H/D isotopologues of *trans*-formic acid. The band centres for each doublet are reported in units of cm^{-1}, where the more intense bands are printed in bold letters. The experimental (exp) value of the Fermi resonance coupling constant $|W_{Fermi}|$ (in cm^{-1}) has been calculated according to eqn (2) and its error bars are computed using Gaussian error propagation with band centre uncertainties of ± 2 cm^{-1} and integrated band intensity errors of $\pm 20\%$. The integrated intensities I are given with respect to the lower-intensity contribution. The calculated (calc) value of the coupling constant has been obtained from the quartic force field of the analytic PES by Tew and Mizukami (see ESI for further details)

						$\lvert W_{Fermi}\rvert$	
System	ν_i	$\tilde{\nu}_{high}$	$\tilde{\nu}_{low}$	I_{high}	I_{low}	Exp	Calc
HCOOH	ν_1	**3570**	3567	3(0.5)	2	2(2)	0.3
HCOOD	ν_2	2954	**2938**	1(0.5)	1	8(2)[a]	8.7
DCOOD	ν_2	**2231**	2194	2(1)	1	17(2)	18.9
DCOOH	ν_3	**1762**	1725	3(0.5)	2	18(2)	18.3
DCOOD	ν_3	**1761**	1725	3(0.5)	2	18(2)	18.1
HCOOH	ν_5	**1306**	1220	7(2)	1	28(4)	39.6
DCOOH	ν_5	**1299**	1206	7(2)	1	31(4)	42.7
HCOOD	ν_5	1010	**972**	1(1)	3	17(2)[b]	16.8
DCOOD	ν_5		**945**				3.3

[a] Only Q branches (without additional substructure) were integrated to determine $|W^{exp}_{Fermi}|$. [b] Determined from a depolarised spectrum (see bottom of Fig. S5 in the ESI).

(*cf.* Fig. 2 and Table 2), so that their contributions to the rotational contour should also be similar. For $\nu_5/2\nu_9$ of HCOOD, there seems to be a broad rotational substructure which cannot be easily disentangled. Therefore, additional depolarisation measurements were performed (Fig. S5 in the ESI†) and $|W^{exp}_{Fermi}|$ was determined from these spectra.

As expected from the small spectral separation $\Delta\tilde{\nu} = 3$ cm^{-1}, the Fermi resonance of ν_1 of HCOOH is the weakest observed in this work with a coupling matrix element $|W^{exp}_{Fermi}|$ of solely 2(2) cm^{-1}. It agrees with the very small predicted value $|W^{calc}_{Fermi}|$ between ν_1 and the $(\nu_2 + \nu_7)$ combination band, although the third band in the Raman spectra and the resonance triad observed in helium nanodroplets[38] indicate a more complex interaction than a simple two level resonance. Also rather weak is the ν_2 Fermi resonance of HCOOD with 8(2) cm^{-1}. Again, $|W^{calc}_{Fermi}|$ and $|W^{exp}_{Fermi}|$ match rather well, which supports the assignment by Bertie *et al.*[5] who ascribed the resonance partner to the $(\nu_3 + \nu_6)$ combination band. The strength of the $\nu_3/2\nu_8$ Fermi resonance observed for the C-deuterated isotopologues is near-identical and accidentally very similar to that of ν_2 of DCOOD (*cf.* Table 2). For all three resonances, the experimental and predicted Fermi coupling matrix elements agree within the experimental error bars.

For the $\nu_5/2\nu_9$ resonance doublet, a distinct strength variation is observed across the four isotopologues – it is largest for DCOOH (31(4) cm^{-1}), decreases from HCOOH (28(4) cm^{-1}) to HCOOD (17(2) cm^{-1}), and remains undetected for DCOOD (*cf.* Fig. 4). As for most other resonance doublets, $|W^{calc}_{Fermi}|$ of HCOOD matches the experimental value within the error bars. The calculated coupling constants $|W^{calc}_{Fermi}|$ of HCOOH and DCOOH are 12 cm^{-1} larger than the experimental values. These findings seem to contradict the assumption of a completely dark state in case of $2\nu_9$ of the two O–H isotopologues (*cf.* eqn (2)). Further investigation of this might be worthwhile. Overall, this is just one of many examples where anharmonic Raman intensities could prove to be very helpful.

4 Conclusions

After over eighty years of experimental research since the first publication on the formic acid monomer (and dimer) by Bonner and Hofstadter in 1938,[32] the vibrational spectra of the simplest carboxylic acid are still not yet fully understood. The most notable missing vibrational information concerns its higher-energy *cis*-conformation, particularly that of the deuterated isotopologues of formic acid, where no perturbation-free band positions were known prior to this work. Recently, Raman jet spectroscopy in combination with thermal excitation was used to increase the number of *cis*-HCOOH fundamentals from one to five.[24] In this work, we have extended this technique to *cis*-HCOOD, -DCOOH, and -DCOOD and were able to assign the bands of all O–H/D, C–H/D, C═O stretching as well as those of the two O–D in-plane bending vibrations.

For the *trans*-formic acid monomer, although all but one fundamental vibration of the H/D isotopologues have already been determined, there is still ambiguity concerning assignments of overtones, combination bands, and Fermi resonance partners.[11,12] A comparison of the latter amongst all four isotopologues has proven to be very insightful, particularly for the $\nu_5/2\nu_9$ resonance. This resonance is found to be weakest for HCOOD and appears to be absent in DCOOD. For HCOOH and DCOOH, similar coupling strengths are predicted, though from our Raman spectra we obtain smaller experimental coupling constants for both. This discrepancy between theory and experiment hints at a more complicated resonance mixing than that of a 'bright' fundamental interacting with a 'dark' overtone. The reason for the absence of this Fermi resonance in DCOOD might be harmonic mode mixing between ν_4 and ν_5 that detunes the resonance, yet for exact conclusions, further theoretical investigation is necessary.

Non-isomeric hot bands (see for example Fig. S2–S5 in the ESI†) are another valuable benchmarking target in addition to the *cis*-fundamentals and the Fermi resonance coupling matrix elements $|W_{Fermi}|$, as these facilitate an analysis of weaker anharmonicity signatures x_{ij}.[24,44] For a thorough analysis of the large number of these hot bands observed in our spectra, a close collaboration between theory and experiment is vital. This represents one of the future directions of this work. The wealth of isomerically hot, yet rotationally cold formic acid monomer data provided in this contribution significantly advances its standing as a benchmarking reference system and hopefully triggers further theoretical investigation on this system.

Conflicts of interest

Ther e are no conflicts to declare.

Acknowledgements

This work was funded by the Deutsche Forschungsgemeinschaft (DFG, German Research Foundation) – 389479699/GRK2455 and 405832858. The authors thank M. Schwarzer for his help with early DCOOD measurements and Z. Xue for a preliminary Raman jet study of the *trans*-formic acid spectra.[31] A. Nejad thanks the Fonds der Chemischen Industrie (FCI) for an attractive scholarship.

Notes and references

1 R. Zander, P. Duchatelet, E. Mahieu, P. Demoulin, G. Roland, C. Servais, J. V. Auwera, A. Perrin, C. P. Rinsland and P. J. Crutzen, *Atmos. Chem. Phys.*, 2010, **10**, 10047–10065.
2 D. B. Millet, M. Baasandorj, D. K. Farmer, J. A. Thornton, K. Baumann, P. Brophy, S. Chaliyakunnel, J. A. de Gouw, M. Graus, L. Hu, A. Koss, B. H. Lee, F. D. Lopez-Hilfiker, J. A. Neuman, F. Paulot, J. Peischl, I. B. Pollack, T. B. Ryerson, C. Warneke, B. J. Williams and J. Xu, *Atmos. Chem. Phys.*, 2015, **15**, 6283–6304.
3 I. C. Hisatsune and J. Heicklen, *Can. J. Spectrosc.*, 1973, **18**, 135–142.
4 J. E. Bertie and K. H. Michaelian, *J. Chem. Phys.*, 1982, **76**, 886–894.
5 J. E. Bertie, K. H. Michaelian, H. H. Eysel and D. Hager, *J. Chem. Phys.*, 1986, **85**, 4779–4789.
6 M. Freytes, D. Hurtmans, S. Kassi, J. Liévin, J. Vander Auwera, A. Campargue and M. Herman, *Chem. Phys.*, 2002, **283**, 47–61.
7 F. Madeja, A. Hecker, S. Ebbinghaus and M. Havenith, *Spectrochim. Acta, Part A*, 2003, **59**, 1773–1782.
8 O. I. Baskakov, E. A. Alekseev, R. A. Motiyenko, J. Lohilahti, V.-M. Horneman, S. Alanko, B. P. Winnewisser, I. R. Medvedev and F. C. De Lucia, *J. Mol. Spectrosc.*, 2006, **240**, 188–201.
9 K. G. Goroya, Y. Zhu, P. Sun and C. Duan, *J. Chem. Phys.*, 2014, **140**, 164311.
10 W. Luo, Y. Zhang, W. Li and C. Duan, *J. Mol. Spectrosc.*, 2017, **334**, 22–25.
11 D. P. Tew and W. Mizukami, *J. Phys. Chem. A*, 2016, **120**, 9815–9828.
12 F. Richter and P. Carbonnière, *J. Chem. Phys.*, 2018, **148**, 064303.
13 A. Aerts, P. Carbonnière, F. Richter and A. Brown, *J. Chem. Phys.*, 2020, **152**, 024305.
14 W. H. Hocking, *Z. Naturforsch., A*, 1976, **31**, 1113–1121.
15 M. Winnewisser, B. P. Winnewisser, M. Stein, M. Birk, G. Wagner, G. Winnewisser, K. M. T. Yamada, S. P. Belov and O. I. Baskakov, *J. Mol. Spectrosc.*, 2002, **216**, 259–265.
16 M. Pettersson, J. Lundell, L. Khriachtchev and M. Räsänen, *J. Am. Chem. Soc.*, 1997, **119**, 11715–11716.
17 E. M. S. Maçôas, J. Lundell, M. Pettersson, L. Khriachtchev, R. Fausto and M. Räsänen, *J. Mol. Spectrosc.*, 2003, **219**, 70–80.
18 A. Domanskaya, K. Marushkevich, L. Khriachtchev and M. Räsänen, *J. Chem. Phys.*, 2009, **130**, 154509.
19 L. O. Paulson, D. T. Anderson, J. Lundell, K. Marushkevich, M. Melavuori and L. Khriachtchev, *J. Phys. Chem. A*, 2011, **115**, 13346–13355.
20 E. L. Sibert III, *J. Chem. Phys.*, 2019, **150**, 090901.
21 F. Ito, *Comput. Theor. Chem.*, 2019, **1161**, 18–25.
22 O. I. Baskakov, V.-M. Horneman, J. Lohilahti and S. Alanko, *J. Mol. Struct.*, 2006, **795**, 49–53.
23 K. A. E. Meyer and M. A. Suhm, *J. Chem. Phys.*, 2018, **149**, 104307.
24 K. A. E. Meyer and M. A. Suhm, *Chem. Sci.*, 2019, **10**, 6285–6294.
25 G. Giubertoni, O. O. Sofronov and H. J. Bakker, *J. Phys. Chem. Lett.*, 2019, **10**, 3217–3222.
26 J. Demaison, M. Herman and J. Liévin, *J. Chem. Phys.*, 2007, **126**, 164305.
27 K. Hull, T. Wells, B. E. Billinghurst, H. Bunn and P. L. Raston, *AIP Adv.*, 2019, **9**, 015021.
28 R. L. Redington, *J. Mol. Spectrosc.*, 1977, **65**, 171–189.
29 L. G. Bonner and J. S. Kirby-Smith, *Phys. Rev.*, 1940, **57**, 1078.
30 A. Olbert-Majkut, J. Ahokas, J. Lundell and M. Pettersson, *Chem. Phys. Lett.*, 2009, **468**, 176–183.
31 Z. Xue, *Raman spectroscopy of carboxylic acid and water aggregates*, PhD thesis, Logos Berlin, Berlin, 2011.
32 L. G. Bonner and R. Hofstadter, *J. Chem. Phys.*, 1938, **6**, 531–534.
33 V. Z. Williams, *J. Chem. Phys.*, 1947, **15**, 243–251.
34 J. K. Wilmshurst, *J. Chem. Phys.*, 1956, **25**, 478–480.
35 R. C. Millikan and K. S. Pitzer, *J. Chem. Phys.*, 1957, **27**, 1305–1308.
36 O. I. Baskakov, H. Bürger and W. Jerzembeck, *J. Mol. Spectrosc.*, 1999, **193**, 33–45.
37 T. L. Tan, K. L. Goh, P. P. Ong and H. H. Teo, *J. Mol. Spectrosc.*, 1999, **198**, 387–392.
38 F. Madeja, P. Markwick, M. Havenith, K. Nauta and R. E. Miller, *J. Chem. Phys.*, 2002, **116**, 2870–2878.
39 A. Perrin, J.-M. Flaud, B. Bakri, J. Demaison, O. Baskakov, S. Sirota, M. Herman and J. Auwera, *J. Mol. Spectrosc.*, 2002, **216**, 203–213.
40 A. Perrin, J. Vander Auwera and Z. Zelinger, *J. Quant. Spectrosc. Radiat. Transfer*, 2009, **110**, 743–755.
41 P. Das, C. J. Knapp and W. Jäger, *J. Mol. Spectrosc.*, 2017, **341**, 17–22.
42 A. Nejad, E. Meyer and M. A. Suhm, *J. Phys. Chem. Lett.*, 2020, **11**, 5228–5233.
43 F. Kollipost, R. Wugt Larsen, A. V. Domanskaya, M. Nörenberg and M. A. Suhm, *J. Chem. Phys.*, 2012, **136**, 151101.
44 T. Forsting and M. Suhm, Curry-Jet SETUP, DOI: 10.6084/m9.figshare.6395840.v1.
45 M. Gawrilow and M. A. Suhm, *Phys. Chem. Chem. Phys.*, 2020, **22**, 15303–15311.
46 K. A. E. Meyer and M. A. Suhm, *J. Chem. Phys.*, 2017, **147**, 144305.
47 M. A. Suhm and F. Kollipost, *Phys. Chem. Chem. Phys.*, 2013, **15**, 10702–10721.

48 M. J. Frisch, G. W. Trucks, H. B. Schlegel, G. E. Scuseria, M. A. Robb, J. R. Cheeseman, G. Scalmani, V. Barone, B. Mennucci, G. A. Petersson, H. Nakatsuji, M. Caricato, X. Li, H. P. Hratchian, A. F. Izmaylov, J. Bloino, G. Zheng, J. L. Sonnenberg, M. Hada, M. Ehara, K. Toyota, R. Fukuda, J. Hasegawa, M. Ishida, T. Nakajima, Y. Honda, O. Kitao, H. Nakai, T. Vreven, J. A. Montgomery, Jr., J. E. Peralta, F. Ogliaro, M. Bearpark, J. J. Heyd, E. Brothers, K. N. Kudin, V. N. Staroverov, R. Kobayashi, J. Normand, K. Raghavachari, A. Rendell, J. C. Burant, S. S. Iyengar, J. Tomasi, M. Cossi, N. Rega, J. M. Millam, M. Klene, J. E. Knox, J. B. Cross, V. Bakken, C. Adamo, J. Jaramillo, R. Gomperts, R. E. Stratmann, O. Yazyev, A. J. Austin, R. Cammi, C. Pomelli, J. W. Ochterski, R. L. Martin, K. Morokuma, V. G. Zakrzewski, G. A. Voth, P. Salvador, J. J. Dannenberg, S. Dapprich, A. D. Daniels, Ö. Farkas, J. B. Foresman, J. V. Ortiz, J. Cioslowski and D. J. Fox, *Gaussian 09 Revision E.01*, 2009.
49 A. D. Becke, *J. Chem. Phys.*, 1993, **98**, 5648.
50 C. Lee, W. Yang and R. G. Parr, *Phys. Rev. B*, 1988, **37**, 785–789.
51 S. Grimme, J. Antony, S. Ehrlich and H. Krieg, *J. Chem. Phys.*, 2010, **132**, 154104.
52 S. Grimme, S. Ehrlich and L. Goerigk, *J. Comput. Chem.*, 2011, **32**, 1456–1465.
53 T. H. Dunning Jr., *J. Chem. Phys.*, 1989, **90**, 1007–1023.
54 C. Adamo and V. Barone, *J. Chem. Phys.*, 1999, **110**, 6158–6170.
55 S. Grimme, *J. Chem. Phys.*, 2006, **124**, 034108.
56 C. Møller and M. S. Plesset, *Phys. Rev.*, 1934, **46**, 618–622.
57 J. Gauss and J. F. Stanton, *Chem. Phys. Lett.*, 1997, **276**, 70–77.
58 J. F. Stanton, J. Gauss, L. Cheng, M. E. Harding, D. A. Matthews and P. G. Szalay, CFOUR, Coupled-Cluster techniques for Computational Chemistry, a quantum-chemical program package, With contributions from A. A. Auer, R. J. Bartlett, U. Benedikt, C. Berger, D. E. Bernholdt, Y. J. Bomble, O. Christiansen, F. Engel, R. Faber, M. Heckert, O. Heun, M. Hilgenberg, C. Huber, T.-C. Jagau, D. Jonsson, J. Jusélius, T. Kirsch, K. Klein, W. J. Lauderdale, F. Lipparini, T. Metzroth, L. A. Mück, D. P. O'Neill, D. R. Price, E. Prochnow, C. Puzzarini, K. Ruud, F. Schiffmann, W. Schwalbach, C. Simmons, S. Stopkowicz, A. Tajti, J. Vázquez, F. Wang, J. D. Watts and the integral packages MOLECULE (J. Almlöf and P. R. Taylor), PROPS (P. R. Taylor), ABACUS (T. Helgaker, H. J. A. Jensen, P. Jørgensen, and J. Olsen), and ECP routines by A. V. Mitin and C. van Wüllen, for the current version, see http://www.cfour.de.
59 D. A. Matthews, L. Cheng, M. E. Harding, F. Lipparini, S. Stopkowicz, T.-C. Jagau, P. G. Szalay, J. Gauss and J. F. Stanton, *J. Chem. Phys.*, 2020, **152**, 214108.
60 P. Huber-Wälchli and H. H. Günthard, *Spectrochim. Acta, Part A*, 1981, **37**, 285–304.
61 H. H. Nielsen, *Rev. Mod. Phys.*, 1951, **23**, 90–136.
62 We note that the hot band $(2\nu_6–\nu_6)$ of *trans*-HCOOH in *Chem. Sci.*, 2019, **10**, 6285–6294 (ref. 24) was incorrectly assumed to be shifted by x_{66} rather than $2x_{66}$ from the ν_6-fundamental. By considering the missing factor of two, the predicted shift of this non-isomeric hot band is similar to the *cis–trans*-shift of ν_6, *i.e.*, it could contribute to the band assigned to ν_6 of *cis*-HCOOH. The expected intensity of the $(2\nu_6–\nu_6)$ hot band, however, is distinctly too small for it to be the sole contribution to the band at 1093 cm^{-1}. As such, the *cis*-HCOOH assignment remains largely unaffected.
63 W. H. Weber, P. D. Maker, J. Johns and E. Weinberger, *J. Mol. Spectrosc.*, 1987, **121**, 243–260.
64 O. I. Baskakov and J. Demaison, *J. Mol. Spectrosc.*, 2002, **211**, 262–272.
65 K. L. Goh, P. P. Ong and T. L. Tan, *Spectrochim. Acta, Part A*, 1999, **55**, 2601–2614.
66 O. I. Baskakov, S. Alanko and M. Koivusaari, *J. Mol. Spectrosc.*, 1999, **198**, 40–42.
67 K. L. Goh, P. P. Ong, T. L. Tan, W. F. Wang and H. H. Teo, *J. Mol. Spectrosc.*, 1998, **190**, 125–129.
68 O. I. Baskakov, J. Lohilahti and V.-M. Horneman, *J. Mol. Spectrosc.*, 2003, **219**, 191–199.
69 R. A'dawiah, T. L. Tan and L. L. Ng, *J. Mol. Spectrosc.*, 2018, **349**, 43–48.
70 O. I. Baskakov, *J. Mol. Spectrosc.*, 2002, **213**, 1–7.
71 L. Nemes, A. R. W. McKellar and J. W. C. Johns, *J. Opt. Soc. Am. B*, 1987, **4**, 1165–1172.
72 K. L. Goh, P. P. Ong, H. H. Teo and T. L. Tan, *J. Mol. Spectrosc.*, 1999, **197**, 322–323.
73 T. L. Tan, K. L. Goh, P. P. Ong and H. H. Teo, *J. Mol. Spectrosc.*, 1999, **198**, 110–114.
74 O. I. Baskakov, *J. Mol. Spectrosc.*, 2001, **208**, 194–196.
75 K. L. Goh, P. P. Ong, H. H. Teo and T. L. Tan, *Spectrochim. Acta, Part A*, 2000, **56**, 991–1001.
76 T. L. Tan, K. L. Goh, P. P. Ong and H. H. Teo, *J. Mol. Spectrosc.*, 1999, **195**, 324–327.
77 D. Luckhaus, M. Quack and M. Willeke, *Z. Phys. Chem.*, 2000, **214**, 889.
78 D. A. Long, *The Raman effect: A unified treatment of the theory of Raman scattering by molecules*, Wiley, Chichester and New York, 2002.
79 S. J. Daunt and H. F. Shurvell, *J. Mol. Spectrosc.*, 1976, **62**, 373–395.